Supplementary Information for:
Intermediate Field Spin(on) Dynamics in α-$RuCl_3$

C. L. Sarkis,[1],* K.D. Dixit,[2,3] P. Rao,[4,5] G. Khundzakishvili,[2] C. Balz,[1,6] J-Q. Yan,[7] B. Winn,[1] T.J. Williams,[1,6] U. Arjun,[2,8] R. Moessner,[9] D.A. Tennant,[10,11] J. Knolle,[4,5] S.E. Nagler,[1,10], A. Banerjee[2,3, †]

[1]*Neutron Scattering Division, Oak Ridge National Laboratory, Oak Ridge, Tennessee, 37831, USA*
[2]*Department of Physics and Astronomy, Purdue University, West Lafayette, Indiana, 47907, USA*
[3]*Purdue Quantum Science and Engineering, Purdue University, West Lafayette, Indiana, 47907, USA*
[4]*Technical University of Munich, TUM School of Natural Sciences, Physics Department, 85748 Garching, Germany*
[5]*Munich Center for Quantum Science and Technology (MCQST), Schellingstr. 4, 80799 Munchen, Germany*
[6]*ISIS Neutron and Muon Source, Science and Technology Facilities Council, Rutherford Appleton Laboratory, Didcot OX11 0QX, United Kingdom*
[7]*Materials Science and Technology Division, Oak Ridge National Laboratory, Oak Ridge, Tennessee 37831, USA*
[8]*Solid State and Structural Chemistry Unit, Indian Institute of Scince, Bengaluru, 56012, India*
[9]*Max-Planck-Institut fr Physik komplexer Systeme, Dresden, Germany*
[10]*Department of Physics and Astronomy, University of Tennessee, Knoxville, Tennessee 37996, USA*
[11]*Department of Materials Science and Engineering, University of Tennessee, Knoxville, Tennessee 37996, USA*

Contents:

1. Inelastic neutron scattering details:

A. Brillouin Zone in a field

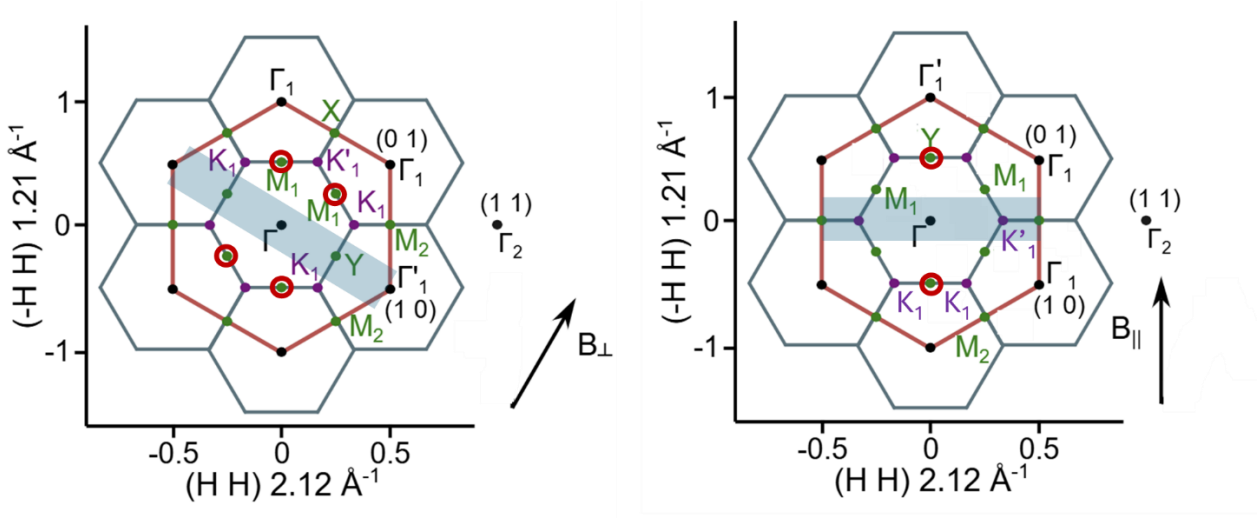

Figure S1: 2D Brillouin Zones in a field and data coverage. *Plots for $B_\perp$ (left) and $B_{||}$ (right) showing the locations of the pseudo-2D locations of the magnetic Bragg peaks and which symmetry point become inequivalent with field. The shaded regions are the locations where we have data coverage from HYSPEC.*

The Brillouin Zones for the crystal structure in Fig 1a of the main article are explained below for two field directions in Fig S1: ***(Left panel)*** When we apply a field greater than 2 T in the ZZ1 phase perpendicular to the bond ($B_\perp$), the system undergoes a domain reorientation transition. Two M_1 points remain equivalent and are represented as just M_1, while the M_1 perpendicular to the applied field is inequivalent and is represented as Y. Similarly, two M_2 points remain equivalent while the M_2 point along the applied field direction is no longer equivalent represented as X. Above 2 T but below B_{C1}, magnetic Bragg peaks appear at the pseudo-M_1 locations with integer L, (shown in red circles,) but not at the pseudo-Y point. ***(Right panel)*** When we apply a field greater than 2 T in the ZZ1 phase parallel to the bond ($B_{||}$), the system again undergoes a domain reorientation transition and the three domains are split into two equivalent domains and on nonequivalent one. Now Y is the M_1 point associated with the domain following the applied field direction and X is associated with the M_2 point perpendicular to the applied field. Above 2 T but below B_{C1}, magnetic Bragg peaks appear at the pseudo-Y location with integer L (shown in red circles), but not at the pseudo-M_1 points. [2]. In the ZZ2 phase, for $B_\perp$, magnetic Bragg peaks appear at the pseudo-Γ point location (0 0 1.5), as well as the pseudo-M1 locations with half-integer L. Pseudo-M1 locations with integer L also retain magnetic Bragg peak intensity from ZZ1. [3]. The blue shaded rectangles depict the approximate data coverages obtained at HYSPEC for our experiment with the typical E_i used in the measurement.

B. HYSPEC Data Acquisition:

Most inelastic neutron scattering data were taken on the direct geometry time of flight hybrid spectrometer (HYSPEC) at the Spallation Neutron Source, located at Oak Ridge National Laboratory. For all HYSPEC measurements, we used a 14 T symmetric vertical field cryomagnet. The magnet has a wedge design, giving a clearance of ±30° within the scattering plane at the center of HYSPEC's detector which was set to an S2 value of -33°. This geometry also restricted our out of plane clearance to roughly ±7.5°. All data shown in the manuscript has detectors masked outside this range to remove additional background arising from the magnet. For all (H 0 L) data, a ^{3}He insert was used and read a base temperature of T = 250 mK. While a ^{3}He insert was originally used for the (H H L) data, a base temperature reading of roughly 1.2 K indicated the insert had a heat leak and was removed to ensure the sample was in equilibrium and held at a constant temperature. The 12 T data taken at E_i = 15 meV presented in the main article still featured the insert and thus shows a different quasielastic shape and background to the rest of the (H H L) data, which was taken with the insert removed and only the main ^{4}He cooling from the cryomagnet. For all preceding measurements the cryomagnet read a base temperature of T = 1.5 K. All fits to data were convolved with intrinsic instrument resolution computed using the Mantid utility *PyChop.*

Neutron scattering experiments with $B_\perp$ were taken on previously measured crystals presented in Ref. [1]. In these experiments the nominal scattering plane was (H 0 L) which allowed for a direct observation of the M-point which corresponds to the onset of zigzag magnetic order, ZZ_1 in zero-field. While magnetic domain reorientations occur at relatively low fields [2], the large out of plane coverage in Ref. [1] was able to track other magnetic Bragg peaks to track the field behavior of the sample and the critical fields.

The neutron scattering experiment with $B_{||}$, such that the scattering plane contains nominally the (H H L) plane was run on a previously unchecked sample. With minimal out-of-plane coverage, observation of the M-point was limited with this experimental setup. Despite this, thanks to the vertical focusing on HYSPEC, we were able to resolve the M-points at the edge of our detectors using E_i = 15 meV. Two magnetic Bragg peaks corresponding to two of the three magnetic domains at (0.5 0 1) and (0 0.5 1) were observed in the low field ZZ_1 ordered phase. Fig. S2a shows the zero-field order parameter scan of the (0.5 0 1) Bragg peak showing a rough onset at the magnetic ordering transition $T_N \sim 7$ K. Observations of the other magnetic Bragg peak corresponding to the 14~K transition at (0.5 0 1.5) were also checked. At T = 8 K we observed no intensity beyond background at the (0.5 0 1.5) Bragg peak after roughly 10 min of counting. Comparing relative intensities of the (0.5 0 1) peak, we constrain the relative fraction of AB-stacking to ≤1% the volume of the sample. Observation of the (0.5 0 1) and (0 0.5 1) Bragg peaks were possible up until a critical field of roughly 1.5 T, at which the system underwent a domain reorientation transition (Fig. S2b). This reorientation left only a single domain whose corresponding magnetic Bragg peaks were completely orthogonal to our nominal scattering plane (along the field direction), eliminating the possibility to directly measure it as an order parameter into the disordered phase.

In the six-layer ZZ_2 phase, neutron diffraction with $B_\perp$ has shown the existence of a very weak magnetic Bragg peak at (0 0 1.5) [3]. While the ZZ_2 phase is expected within a much smaller field range with $B_\perp$, due to a combination of coarse field steps and the low intensity of the peak, we were unable to resolve the onset of the disordered phase within our experiment. Therefore, for the paper, we infer the disordered transition from previous angular dependent susceptibility measurements taken with similarly

grown crystals. They are described in Ref. [3] which show the ZZ_2 transition at ~7.3 T and the disordered transition at ~7.6 T.

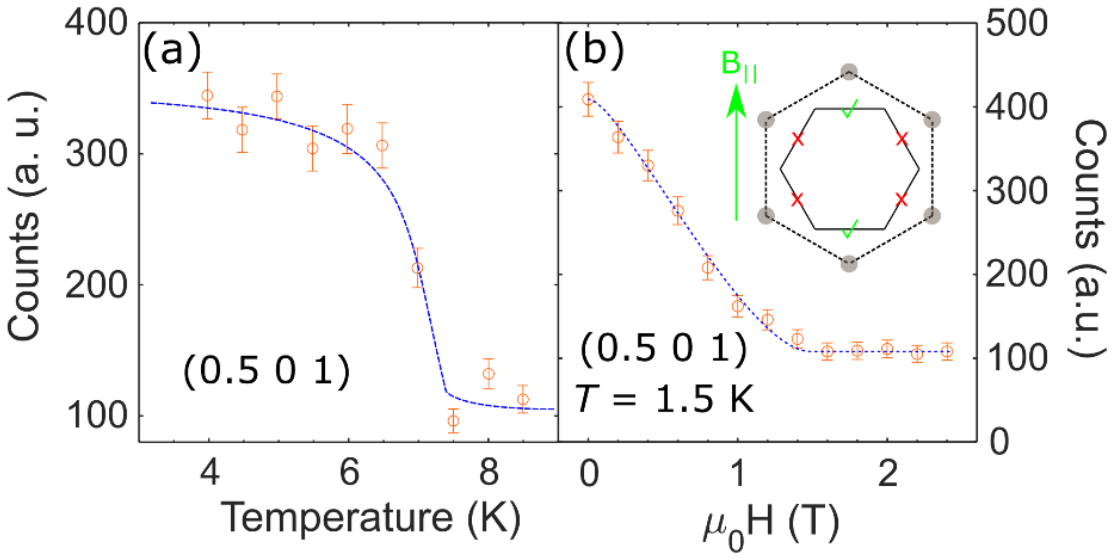

Figure S2: Order Parameter Plots. *(a) Zero-field order parameter of crystal used in $B_{||}$ experiment. The (0.5 0 1) M-point corresponding to the 3-layer ABC stacking was captured near the edge of detectors for E_i = 15 meV and show an onset around T_N = 7 K. (b) Field evolution of the (0.5 0 1) M-point. Above a field of roughly 1.5 T, a magnetic domain reorientation destroys two of the three domains, leaving the only domain corresponding to the field direction left (inset).*

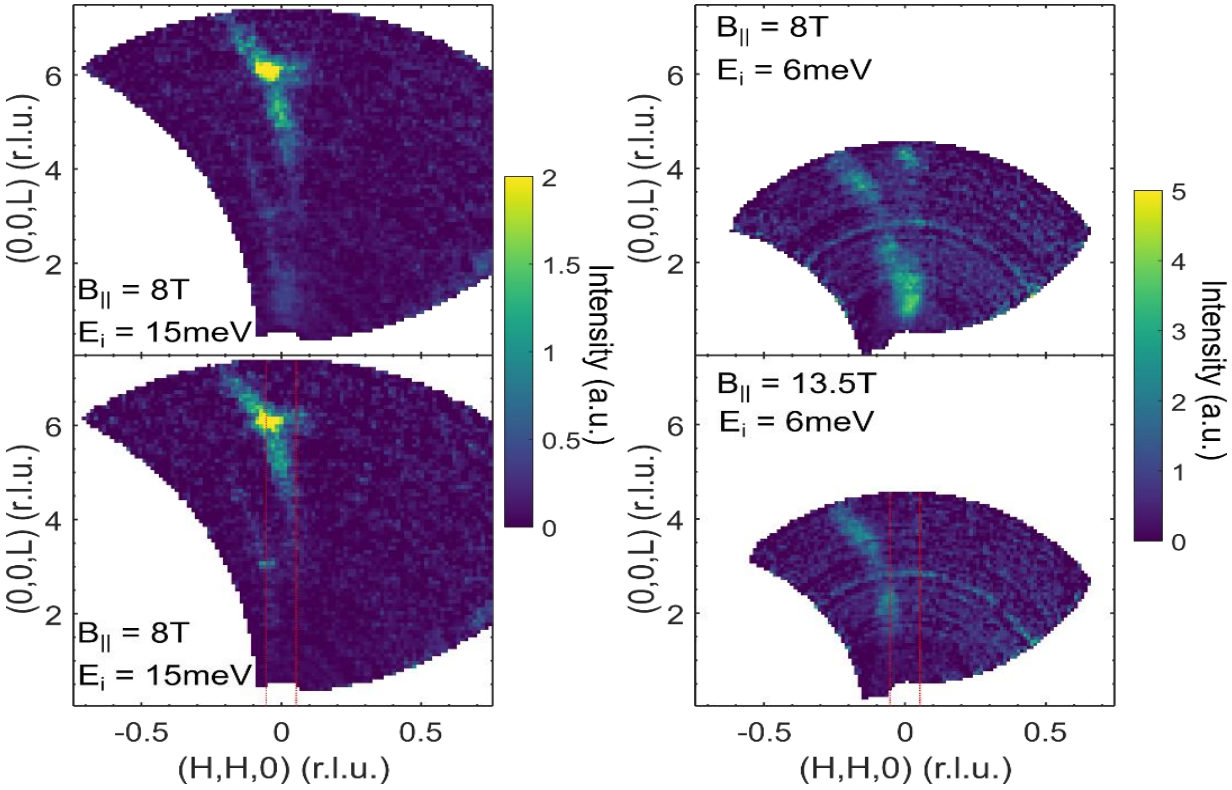

Figure S3: Low energy feature for $B_{||}$. *Constant energy Pseudocolor plots taken with energy integrated ΔE:[1:2]meV. On the left we show the 15meV data taken while the right data show 6 meV data. At 8 T, both datasets show the quasi 2D magnetic continuum centered at (0 0 1.5) and (0 0 4.5) which are pushed up in energy and out of our integration range by 13.5 T. Alongside the magnetic features, large arcs of scattering are observed near, but not centered on (0 0 L) Bragg peaks. The red lines show the integration range used for (0 0 L) vs ΔE plots presented in the main article and below in this document. Because the arcs deflect away from (0 0 L) at higher Q, the integration shows a significant overlap on the low-Q side of Bragg peaks.*

C. Spurion Analysis:

As mentioned in the main article, for Ei = 15 meV and $B_{||}$, we see two field independent features in slices taken along the out of plane momentum transfer. One is a sharply dispersing mode coming out of the (0 0 6) Bragg peak which is within our instrument resolution and naturally corresponds to an acoustic phonon. We discuss the other feature here in more detail here. Shown in Fig. S3, the feature appears in both E_i =15meV and E_i =6meV datasets as arcs of scattering centered just above the elastic line at approximately 1.5 meV. These arcs appear at momentum transfers near, but not above nuclear Bragg peaks (0 0 6) and (0 0 3), respectively.

Interestingly the features do not appear to move for different configurations, with the same arc near (0 0 3) appearing in the same location for both energies. These features do not appear to change as a function of field, indicating they are not related to the magnetism in this material. The scattering is not present during an empty measurement and is thus attached to the sample. The low energy offset and proximity to bright Bragg peaks is consistent with a multiple scattering event.

The feature is responsible for the low energy diffuse scattering observed on the low-Q side of (0 0 L) plots, presented in the main article (Fig. 3) for Ei = 15 meV as well as Fig. S13 below for Ei = 6 meV. In Fig. S2, we note with red dashed lines the integration range used along (H H 0) in our data. Because the arcs deviate from being near (0 0 L) on the high-Q end of the Bragg peak, our integration catches the signal for low-Q but not for the high-Q side of the Bragg peaks. This results in a low energy diffuse signal which appears near the minimum in the magnetic spectra.

Figure S4 depicts the evolution of spin excitation along the in-plane direction (H 0 1.5) without the empty subtraction. As seen in the main text, for higher fields (10 T and above), the excitations are sharper with a more magnon-like behavior but at the lower fields of at $B_\perp$ of 7.3 T and 8 T, a continuum of excitations is observed, with its center near the putative Γ point (H=0). The significant difference in excitations between 8 T and 10 T suggests that the sample may undergo a phase transition somewhere between these fields.

The orange circles in Fig. S4a,g highlight spurious features that are present in all data sets taken with an incident energy of 5.5 meV. These features can be safely ignored for our purposes, as they are likely due to experimental artifacts. The absence of these features in the 12 T data set, which was taken with a different incident energy, confirms that they are indeed spurious. Measurement of an empty angle independent run, where the scattering of the cryomagnet alone was subtracted to all main figure data and was able to clear most of the spurious features shown below.

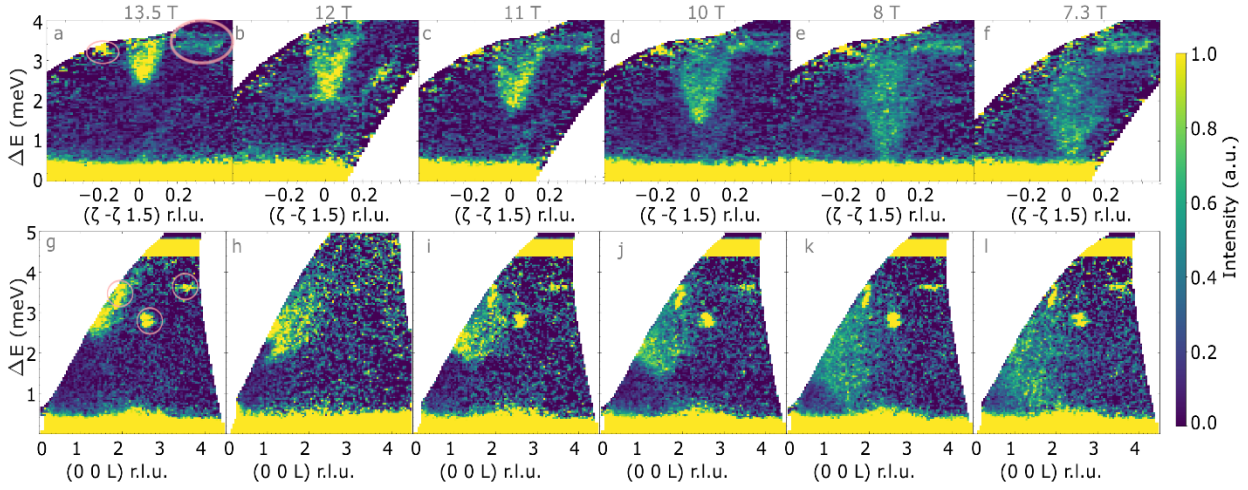

Figure S4: Evolution of continuum for $B_\perp$. *INS raw data without empty - background subtraction taken at T = 0.25 K with E_i = 5.5 meV throughout the intermediate and high-field limit. (a-f) In-plane momentum, (H 0 1.5), vs energy transfer (ΔE) pseudo-color plots. (g-l) The corresponding out-of-plane momentum (0 0 L) vs energy transfer pseudo-color plots. Data show the continuum-like magnetic excitations exhibit a weak minimum near (0 0 1.5) with strongly dispersing in-plane behavior.*

2. **Spin gap analysis using three different methods:**

   A. **Method 1, Linear Dirac dispersion:** To deduce the spin gap using the first method, we assume a Dirac cone-like behavior at the Γ point with a linear density of states, and fit the constant-Q data using a function that solves for the cross point of two straight lines. The first line is fixed at y=0, while the second line is defined as y=m(x-x0). The fitting parameters are m and x0. This approach is based on the idea that the intensity of the mode near the Γ point decreases to zero at low energy, and the gap is represented as the onset of intensity of the mode. The results obtained from this method are summarized below in Table S1.

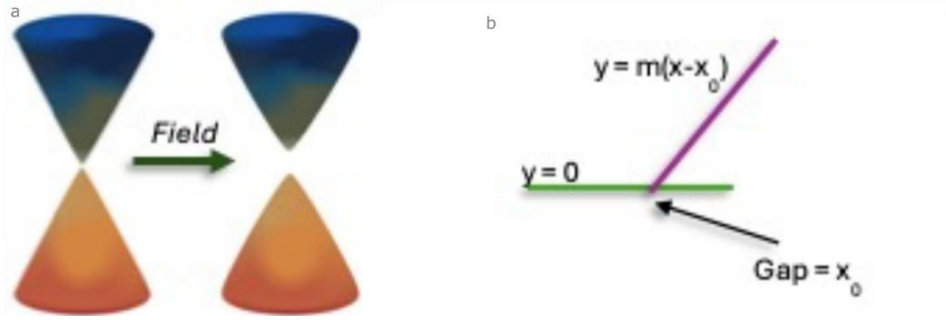

Figure S5: Method 1 - a linear onset of intensity at a Dirac cone type dispersion. *(a) Dirac cone like DOS in a field (b) the fitting routine used to extract a gap by fitting the data to a function that solves for the intersection of two lines: one line is y=0 and the other line is y=slope*(x-x₀). The value of x₀ is defined as the gap. This method is motivated by the assumption that if the density of states follows a Dirac cone-like behavior, then this is a good representation of the gap. The results are below shown for representative 7.3, 8.0 and 10 T, respectively (left to right).*

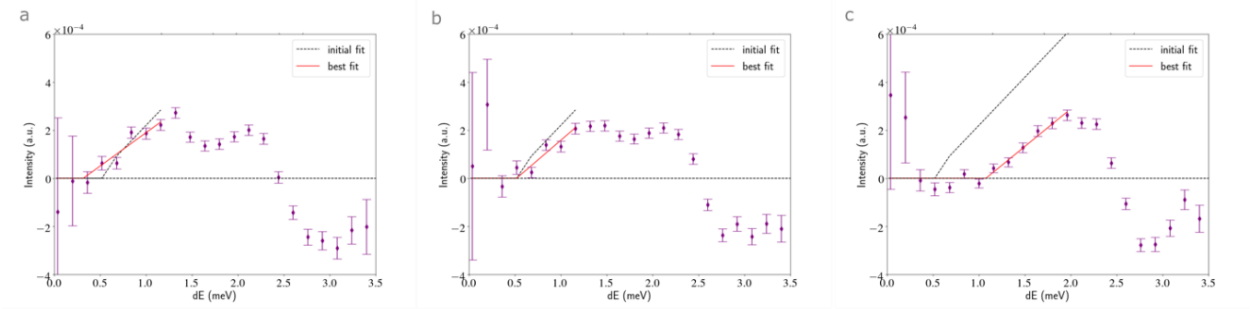

Table S1: Results of onset of intensity analysis: Results with/without the 13.5 T background subtracted.

Field (T)	Fitted Gap (meV)		
7.3	0.31	±	0.11
8	0.52	±	0.19
10	1.16	±	0.10
10 w/o bkg	1.31	±	0.08
11	1.64	±	0.13
11 w/o bkg	1.64	±	0.14
12 w/o bkg	1.78	±	0.10
13.5 w/o bkg	2.28	±	0.07

B. Method 2, Sharp Singularity: If the density of states does not follow a Dirac cone-like behavior, then the inflection point of the intensity of the excitation is a better representation of the gap. To obtain this, the data is fitted to a step function indicating a situation where the bottom of the mode is a sharp bound state or a magnon or a van-Hove singularity. The lmfit.py model has three parameters: amplitude, center, and sigma. The amplitude parameter controls the height of the step function, while the center parameter controls the position of the step edge. The sigma parameter controls the width of the step edge. There are four choices for the form of the step function: linear, arctangent, error, and logistic. The linear form is the default and is the simplest form. The arctangent form is a more gradual transition than the linear form. The error is a more realistic form that considers uncertainty in the data. The logistic form is a more complex form that can be used to model more complex data sets. We use the arctan broadening, and the center of the step function is defined as the gap.

Table S2: Results of inflection point analysis: Results with and without the 13.5 T background subtracted.

Field (T)	Fitted Gap (meV)		
7.3	0.74	±	0.80
8	0.81	±	0.05
10	1.45	±	0.03
10 w/o bkg	1.47	±	0.08
11	1.83	±	0.06
11 w/o bkg	1.86	±	0.12
12 w/o bkg	1.95	±	0.05
13.5 w/o bkg	2.55	±	0.05

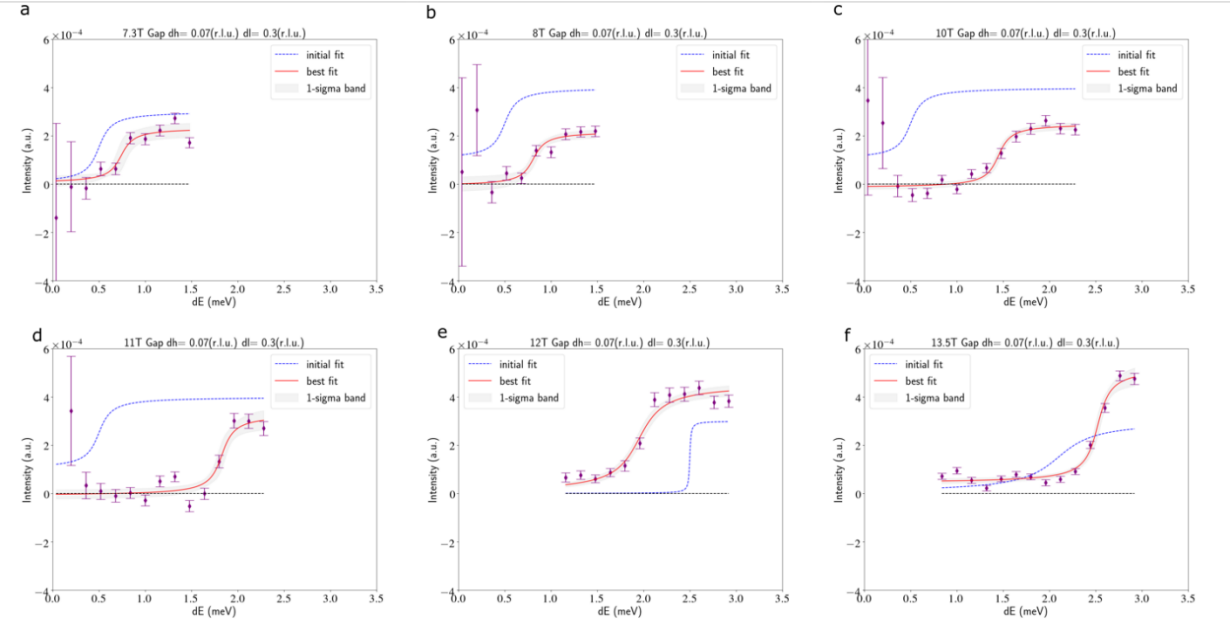

Figure S6: Method 2 – fitting a *tanh* onset at a van-Hove point with spread from resolution effects. *The fitting routine is shown superimposed on the Constant-Q cuts for the fields 7.3 T to 13.5 T. For the lower four fields, the 13.5 T subtracted constant q cuts are used. For 12 T and 13.5 T, the un-subtracted constant Q cuts are used to extract the gap.*

C. **Method 3, Dispersions of Kitaev Model:** Finally, we attempted to fit the dispersion relation in the Kitaev paper relating the spectral gap with the energy.

$$\epsilon(q) \approx \pm\sqrt{(3J^2|\delta q|^2 + \Delta^2)}.$$

We took constant energy cuts of the data for each field and fit each cut to a step function with broadening. This allowed us to find the inflection point of the mode in the direction along the momentum vector (H,0,0) (r.l.u.). We then fit these points to the dispersion relation: The Kitaev interaction term is allowed to vary and values of Δ found from these fits are included in Figure 4 of the main text.

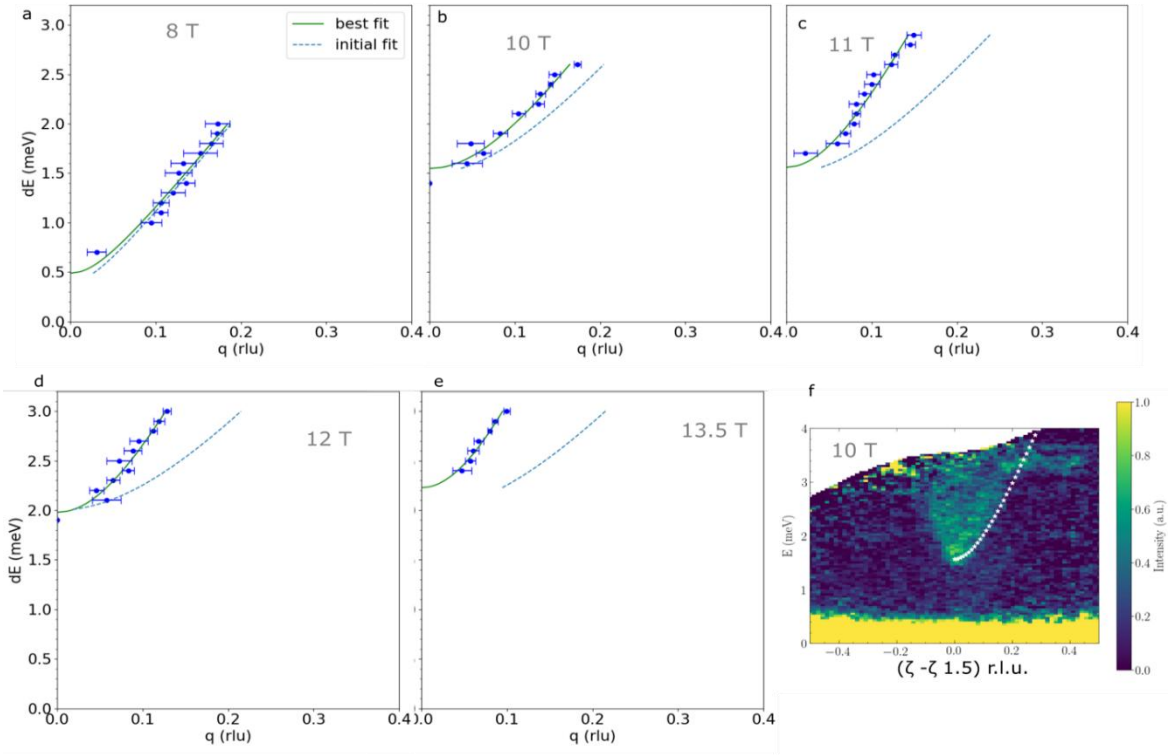

Figure S7: Method 3 – fitting the data to the Kitaev dispersion relation. *We first take constant energy cuts for each field various energies with momentum binning of [-1.5,0.015,1.5] in (H 0 0), integration ranges given by K = [-0.07,0.07], L = [1.2,1.8] and ΔE = ±0.1 meV. These cuts are then fit to a step function with broadening as defined in the lmfit library. This helps us get the values for the edge of our dispersion as seen in (f). Which is then fit to the Kitaev dispersion relation to get the values of J and delta for each field (a-e).*

The onset of intensity method consistently underestimated the gap, while the inflection point method consistently overestimated the gap. The evolution of the gap at the local minima (0 0 1.5) as a function of applied field with $B_\perp$ is summarized in main text Figure 1. Although a non-zero spin gap was observed at a field strength of 7.3 T ($B_\perp$), the amount of data collected at this field was limited, therefore making it uncertain whether a gap truly exists at this field. Non-zero spin gap values were also observed at all other field strengths, and these values are likely to be more accurate. For field strengths of 10 T and 11 T ($B_\perp$), the gap values obtained from the subtracted datasets and the datasets without background subtraction displayed a high degree of agreement.

Table S3: Results of Kitaev dispersion analysis: Results without the 13.5 T background subtraction.

Field (T)	Fitted Gap (meV)		
7.3	no fit		
8	0.43	±	0.14
10	1.57	±	0.03
11	1.68	±	0.04
12	1.98	±	0.05
13.5	2.23	±	0.06

3. Variation of the extracted gap with momentum integration ranges

The value of spin gap can be sensitive to momentum integration ranges[4]. To avoid the gap being substantially overestimated or misdiagnosed, we extract the spin gaps for various in-plane and out-of-plane binning. We show here that our fits to the extracted gap in Section 2 (Method 1) is independent of the momentum integration ranges. Similar outcome is expected for Methods 2 and 3.

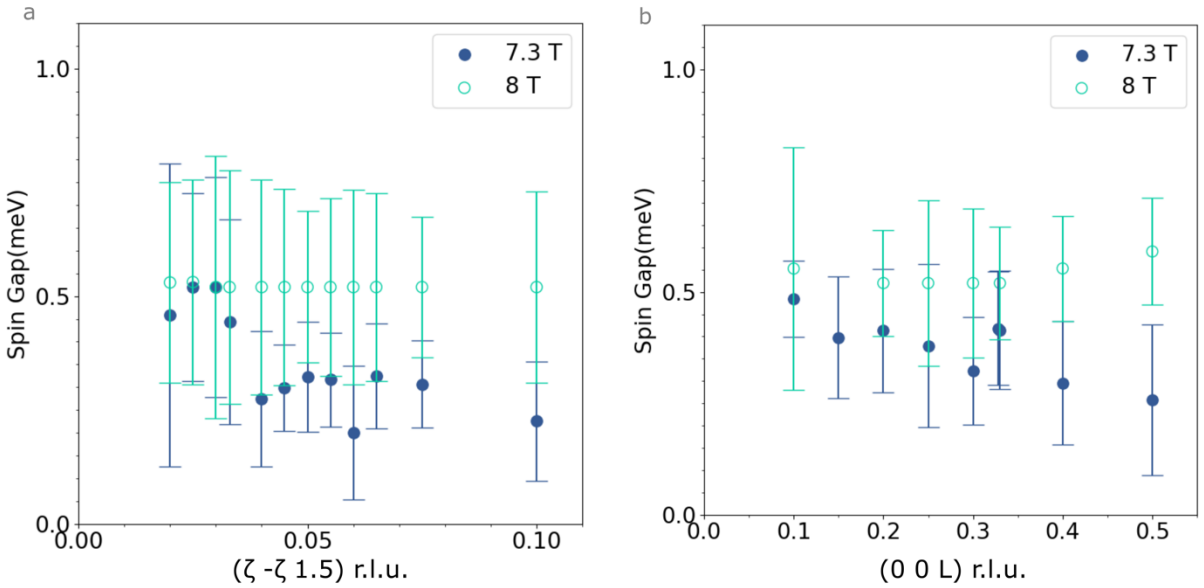

Figure S8: Effects of the gap as a function of momentum integration. *The spin gap was extracted using Method 1 (Section 2) for various momentum binning in both the in-plane and out-of-plane directions. The binning in (H 0 0) direction was held equal to the binning in (0 K 0) direction. (a) spin gap for different (H 0 0) binning for fields 7.3 T and 8 T, (b) spin gap for different (0 0 L) binning for fields 7.3 T and 8 T. We do not see any trend for (H 0 0) binning bur for the out-of-plane direction a binning of 0.3 r.l.u. gives low errors for both 7.3 T and 8 T. Error bars represent the one sigma error obtained from the fitting routine.*

4. Evolution with field: Fits to constant Q cuts of Ei = 15 meV, $B_{||}$ data.

We performed detailed analyses using constant-Q cuts (Figure S9) with 0.15 meV energy binning to quantify the coexistence of the continuum with the bound states. Although not physically motivated, for the sake of completeness, an attempt to still fit the features to two gaussian magnon modes and a gaussian continuum is presented in Fig. S10, showing the evolution of the sharper features with field. The data points

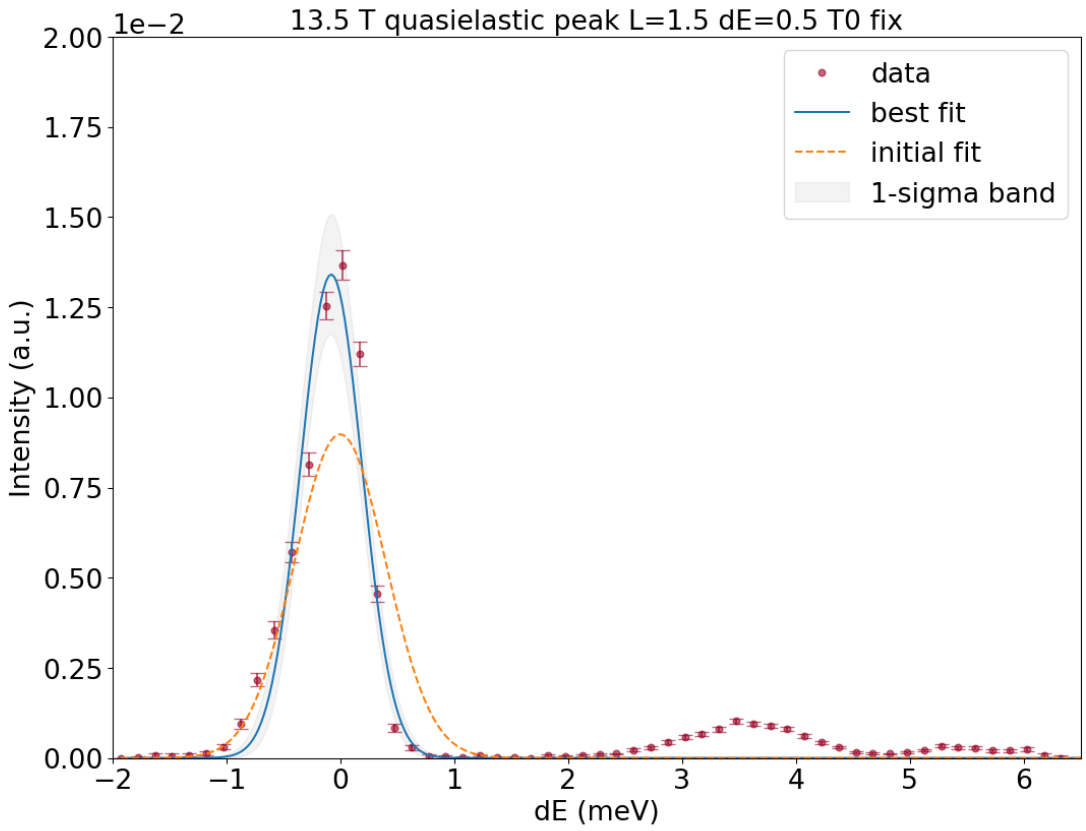

Figure S9: Quasielastic width fitting for $B_{||}$ = 13.5 T for data cuts with smaller energy binning. *The data shown has been integrated over a constant momentum volume in the following ranges: $\Delta\xi$ = [-0.04, 0.04] (r.l.u.), $\Delta\zeta$ = [-0.07, 0.07] (r.l.u.), and ΔL = [1.2, 1.8] (r.l.u.). Energy was binned at 0.15 meV. The center of the gaussian was found to be at E = 0.22(3) meV with a FWHM of 0.60(5) meV.*

are given by pink dots. The data was fitted with a Gaussian peak to characterize the quasi-elastic scattering (blue) centered around 0 meV. The resulting fit was subtracted from the data points, and the residual was fitted again with a broad Gaussian to capture the continuum (grey) observed for 7 T - 10 T. Additionally, two more Gaussian peaks were fit to model the sharpening of the spectrum associated with the magnon-like modes (7.5 T - 13.5 T). The full width at half maximum (FWHM) of both peaks was fixed to be the same, based on the behavior observed in the data. The combined fitting function is given by the blue line. However, a continuum could not be fit for the 12 T and 13.5 T data. Remarkably, the bound states persist down to 7.5 T. It should be noted that for some fields, the error bars on the fit parameters are quite large,

indicating that these fits are not statistically robust. As such, these fits are primarily used as guides to the eye and heuristic approximations rather than definitive quantitative models.

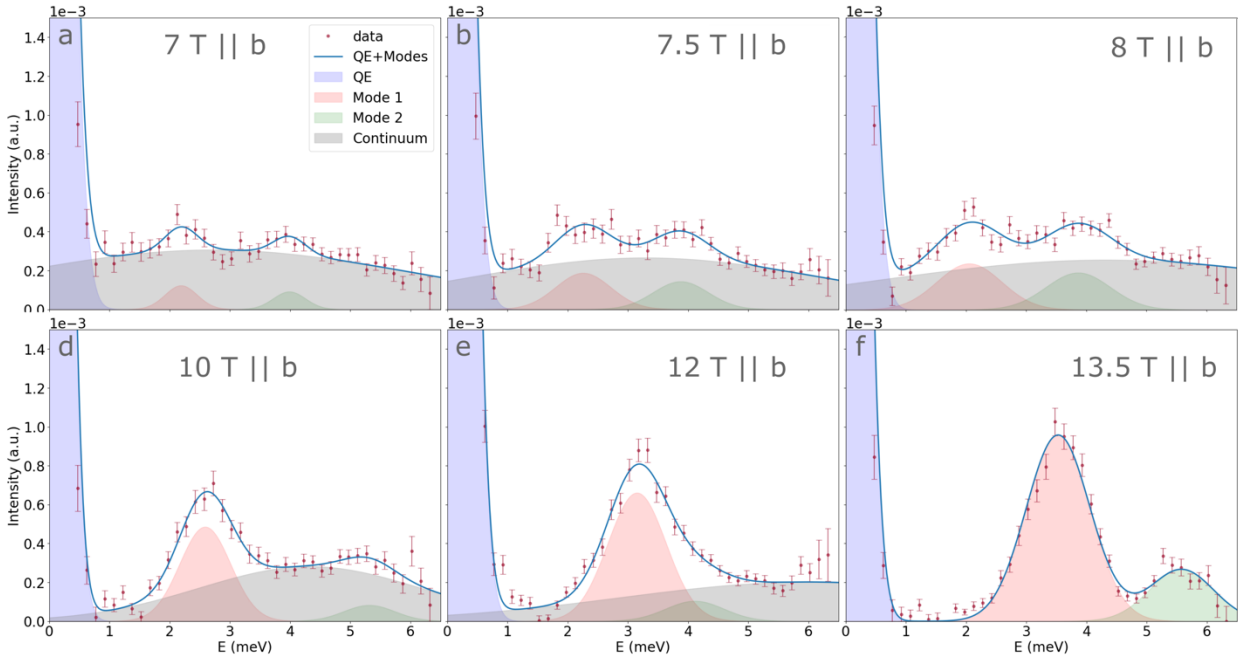

Figure S10: Alternate fitting to capture continuum and bound states for $B_{||}$ for data cuts. *Momentum integrated cuts centered at (0 0 1.5) as a function of field. As field is increased, the system undergoes a smooth collapse of the two sharp and well-ordered magnon-like modes into a broader continuum. Data appears to show that the continuum co-exists with the sharper modes. (a)-(f) show the energy dependence of the scattering, including Gaussian fits to the quasi-elastic scattering, magnon modes, and the broad continuum. The data shown has been integrated over a constant momentum volume in the following ranges: [H,H,0] = [-0.044, 0.044] (r.l.u.), [H,-H,0] = [-0.091, 0.091] (r.l.u.), and [0,0,L] = [1.25, 1.75] (r.l.u.). Energy was binned at 0.15 meV.*

Table S4:

Field (T)	Mode 1 center	stderr	Mode 2 center	stderr	Mode FWHM	stderr	Continuum center	stderr	Continuum FWHM	stderr
7	2.193	0.078	3.992	0.087	0.631	0.182	2.713	0.354	8.014	1.505
7.5	2.261	0.093	3.881	0.086	1.078	0.25	3.301	0.339	7.064	2.414
8	2.076	0.089	3.875	0.070	1.325	0.185	5.715	2.273	12.872	0.880
10	2.593	0.033	5.32	0.185	0.997	0.09	4.331	0.309	4.338	0.52
12	3.154	0.076	4.115	0.386	1.141	0.133	6. 000	0.132	7.302	1.203
13.5	3.528	0.020	5.579	0.07	1.249	0.036	-	-	-	-

Table S5:

Field (T)	Mode 1 Amplitude	Stderr	Mode 2 Amplitude	Stderr	Continuum Amplitude	Stderr
7	8.200e-05	3.10e-05	6.10e-05	2.6e-05	2.61E-03	3.98E-04
7.5	2.14E-04	1.07E-04	1.64E-04	1.00E-04	1.99E-03	3.77E-04
8	1.28E-04	3.80E-05	8.20E-05	2.90E-05	2.19E-03	1.64E-04
10	5.14E-04	5.70E-05	8.70E-05	4.90E-05	1.30E-03	1.67E-04
12	8.02E-04	1.26E-04	1.25E-04	8.60E-05	1.57E-03	3.13E-04
13.5	1.274e-03	4.30e-05	3.55e-04	3.1e-05	-	-

We additionally plot the evolution of the M_1 and M_2 peak positions with field in Fig. S11. The blue dots represent the lower energy magnon peak and the purple dots represent the higher energy magnon peak. *From this evolution, we can extract an effective g-factor* by fitting these data points to straight lines, to find slopes of 0.262 +/- 0.003 and 0.459 +/- 0.027 for the blue and purple lines, respectively. For reference, we also plot the expected Zeeman-like behavior for J = 1 (red line) as well as J = 2 (green line). If we assume J = 1, this leads to a g-factor of (using $E = -g\mu_B J_z B_z$) 3.200 +/- 0.037 for M_1 and 5.607 +/- 0.330 for M_2, respectively. These values seem to disagree with the putative g-factor of ~2 (and ~4) to be expected for a natural separation due to a Zeeman field for a 1-magnon (2-magnon or 2nd harmonic magnon branch).

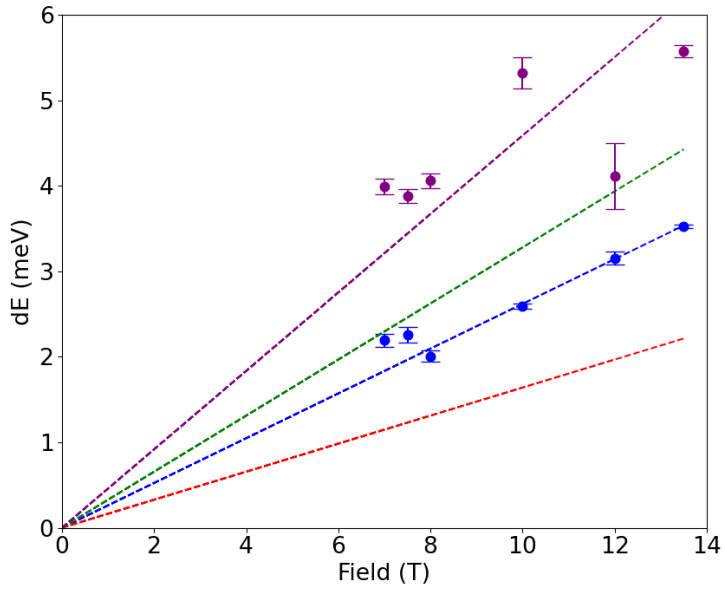

Figure S11: Peak centers from the fits given in Figure S10. *representing the lower energy magnon peaks in blue, higher energy magnon peaks in purple. Dashed lines represent straight line fits to the data points. The green and red lines are for Lande g = 1 and 2 respectively.*

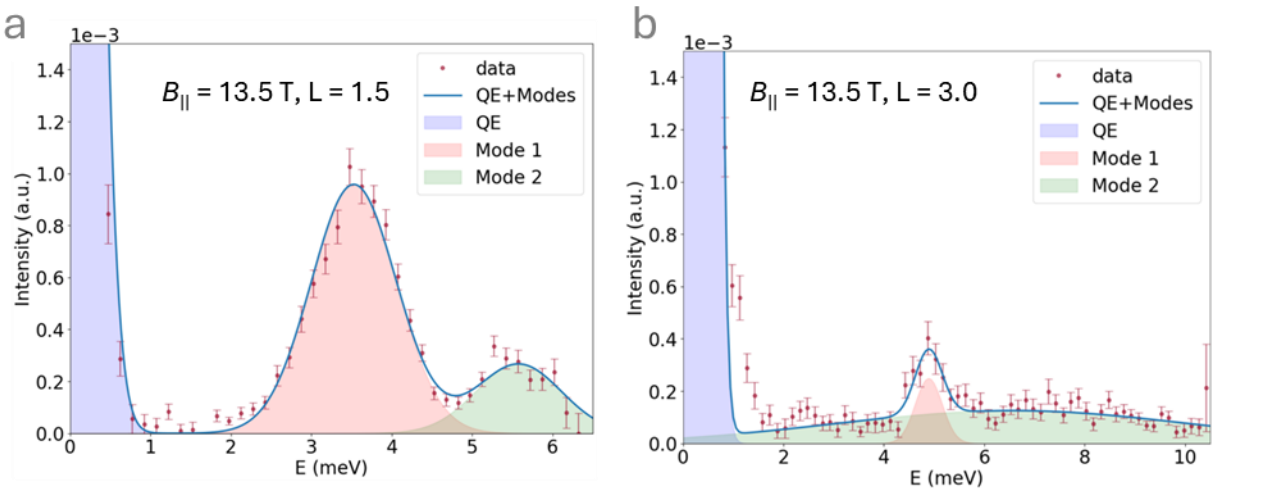

Figure S12: fitting for $B_{||}$ = 13.5 T to capture continuum and bound states for L = 1.5 (a) and L = 3 (b). *Figure depicts both the modes M_1 and M_2 shifting to higher energies at L = 3 as compared to L = 1.5 which agrees with the cosine-like behavior seen in Ref 15.*

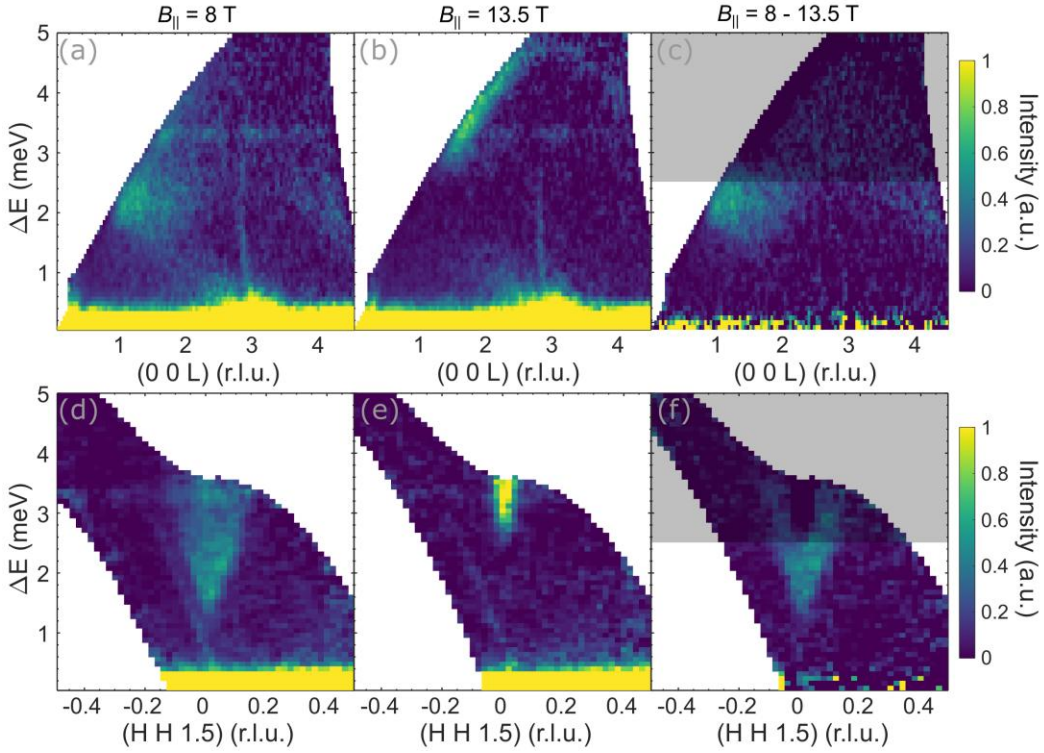

Figure S13: Raw data and high field subtraction for $B_{||}$ and Ei = 6meV on HYSPEC. *Along with the mode, background features observed are smoothly removed using the 13.5T data. Despite being near B_{c2}, the data at 8T shows a clear dispersion in the out of plane plots.*

5. Analysis of Linewidths at the bottom of the band at (0 0 1.5) at 13.5 T

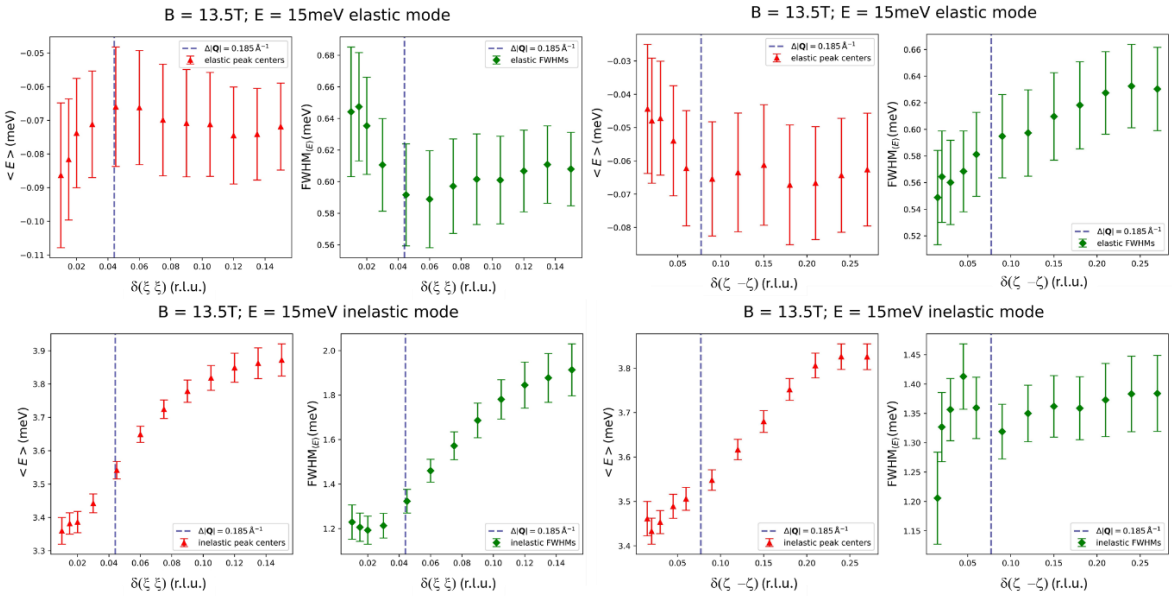

Figure S14: The analysis of the widths of the bottom of the band at (0 0 1.5). *Cuts were performed with different widths in both (x x) and (z -z) directions on the HYSPEC 13.5 T data with Ei = 13.5 meV to study the effects of integration ranges on the linewidths and center of the band. The lowest Q points can come from variability of the Q resolution. We ultimately settled on dQ = 0.184 (blue line) roughly 3 times the momentum resolution for HYSPEC at E_i = 13.5 meV. We show that this represents an optimum point where the (Full-Width at Half-Maximum) FWHMs have converged to within ~5% variation. We note that the elastic width is higher than the native measurement resolution of δE = 0.40(5) meV at E_f = 0, and even finer, 0.35(5) meV at E_f = 3meV. Given the direct geometry of HYSPEC, the resolution at E = 3.3 meV is even better than δE = 0.55(5) meV which we estimate to be roughly δE = 0.35 meV.*

We conclusively show that FWHM of the mode at (0 0 1.5) is 1.22(5) meV which is more than twice the elastic linewidth 0.55(5) meV.

6. Heat Capacity Discussion:

Our extrapolated heat capacity measurements down to T = 1.7 K (Fig. S14), are broadly in agreement with Ref. [6] – that the spin behavior is gapped (gapless) for $B_{\perp}$($B_{||}$). Their thermodynamic gap reported for $B_{\perp}$ at 8 T (7 K = 0.6 meV) is identical to our gap, indicating that we are also probing the same excitation. However, their results contrast the gap obtained from the neutron data for $B_{||}$. This makes the most plausible hypothesis that the gap closes elsewhere in the Brillouin zone where we do not have data coverage. Due to the vertical focusing of HYSPEC and the mostly in-plane detectors operating in a quasi-triple-axis mode, our data coverage is mostly in the scattering plane, which is perpendicular to the applied field. The details of the coverage are presented in Fig. S1, marked by the blue shaded area. As described in Section 1, in a magnetic field the three K and M points are rendered inequivalent and the coverage of this experiment is limited. Thus, we can access only one of the three 2nd BZ M-points (only the one in the scattering plane). None of the 2nd BZ K-points are accessible in our experiment. Hence, our HYSPEC data captured the Y points, but it missed all the K1 and M1 points for $B_{\perp}$ and both M1 and Y points , as well as four out of the six K points for $B_{||}$. Our data also missed all the high symmetry points for the second BZ, other than the Γ point. It cannot be thus ruled out that there could be a location where the spin gap actually closes, which requires future high-resolution measurements away from the Γ point. Importantly, since the magnetic domain reorientation shows a suppression of two out of three magnetic domains, with the only remaining domain oriented along the field producing spectral intensity out of the measurement plane it is possible that the gap closes along the field direction which we cannot rule out. However, such measurements are difficult using neutron scattering because of the Ru^{3+} form factor.

Some discussion on gapless unknown feature at (0 0 5) seen in Ei = 15 meV data is given in Section 2 – we believe this feature is a spurion and does not represent a gapless mode, as it is not field dependent, and does not come off any high symmetry locations of the 2D BZ of $RuCl_3$.

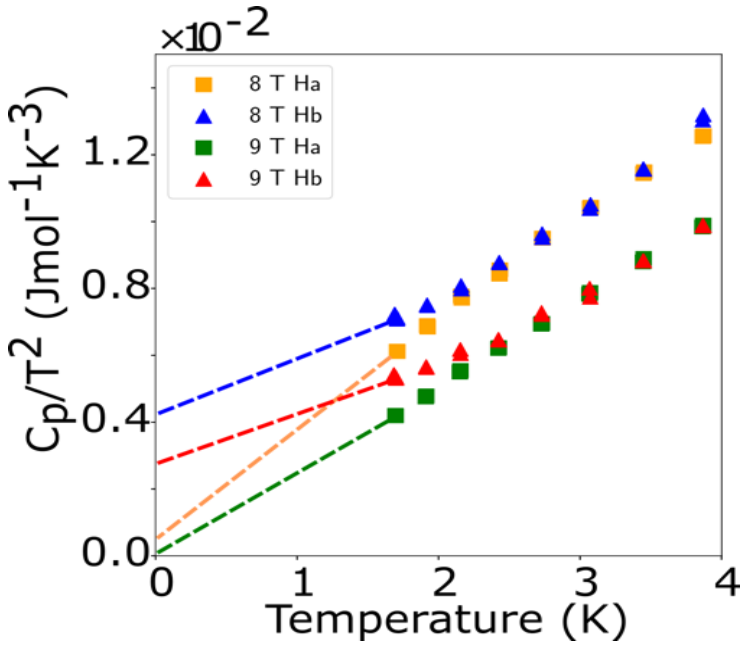

Figure S15: Energy transfer vs applied magnetic field as a pseudo color plot for $B_{\perp}$ (a) and $B_{\parallel}$ (b) respectively. *C_p/T^2 vs. T plots of α-$RuCl_3$ taken at 8 T and 9 T with applied fields both for $B_{||}$ and $B_{\perp}$. Extrapolating back to 0 K, we see evidence of a gapped behavior to the low energy excitations for $B_{||}$, while $B_{\perp}$ appears gapless. The results down to 1.7 K are consistent with those in Ref [40].*

7. Intermediate field induced phase for $B_{||}$

The field-induced mixed phase with 3-layer and 6-layer zigzag antiferromagnetic ordering has been well documented for external fields applied within the honeycomb planes and perpendicular to Ru-Ru bonds. To date direct evidence of the same field induced phase for field applied parallel to a Ru-Ru bond has yet to be reported. While no magnetic Bragg peaks at (0 0 1.5) were observed in the HYSPEC measurements, data taken on the cold triple axis (CTAX) instrument presented in Fig. S16 show a pronounced increase in elastic intensity for 7.5T when compared to 8T and 0.1T. The increased intensity appears robust, showing a higher signal both for measuring after increasing the field from below ZZ2 and after lowering the field from 8T.

One clear question would be why no peaks were observed on HYSPEC. While we do note the Bragg peaks appear weak and may have been concealed in the background, it may also be that the development of ZZ2 for B|| is more sample dependent. Alternatively, the small 1.5deg offset of the scattering plane in the case of HYSPEC data may have been enough to change the field induced behavior.

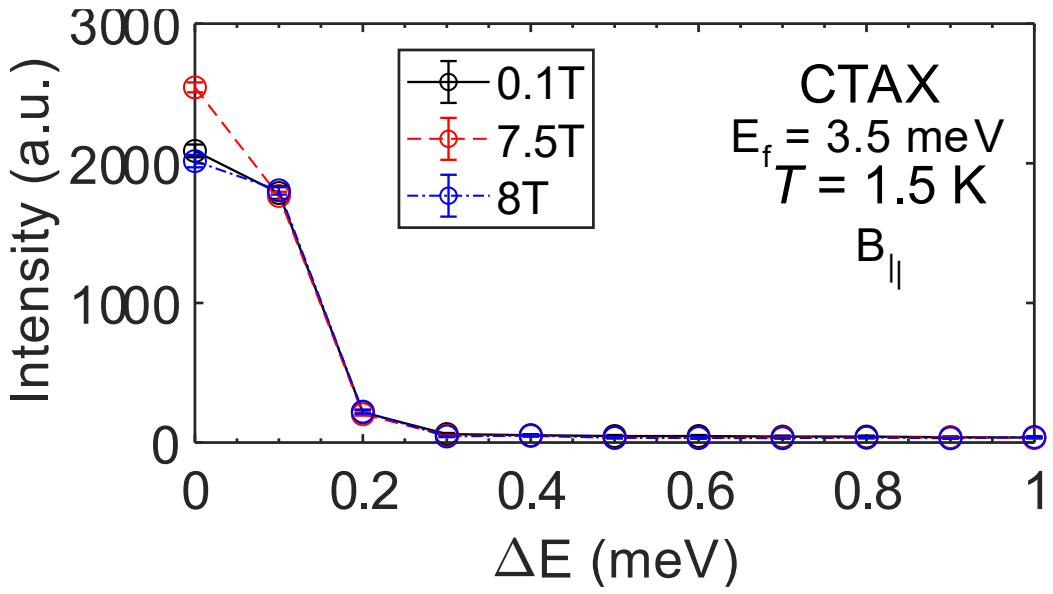

Fig. S16: Evidence for ZZ2 phase for $B_{||}$. *Momentum integrated cuts taken at (0 0 1.5) on CTAX. A higher intensity is observed at the elastic line for 7.5T over both 0.1T and 8T, supporting the development of Bragg peaks at (0 0 1.5) associated with ZZ2.*

8. Two-magnon and multimagnon scattering

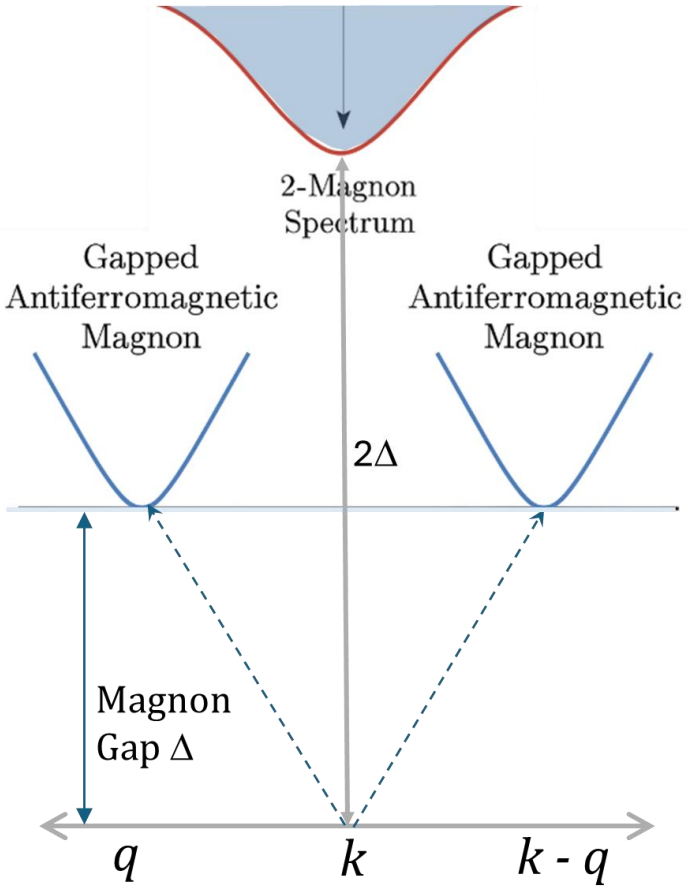

Figure S17: Multimagnon scenario at (0 0 1.5). *A cartoon of the kinematic scattering process* $\epsilon_{\{\omega,k-q\}} + \epsilon_{\{\omega,q\}}$ *with a gap* Δ *leading to a broad 2-magnon continuum at 2-magnon gap* 2Δ *with clear kinematic constraints providing a distinct connection to their momentum dependance.*

In this section we discuss the location of the magnons in α-$RuCl_3$ in the ZZ1 and ZZ2 phases which could lead to a multimagnon continuum. At the B_{C2} transition, the magnons are expected to have a minimum at the corresponding Bragg momenta. With increasing field the magnons slowly start to produce a gap which ultimately would become a linearly-scaling Zeeman gap far from the transition.

In the ZZ1 phase, the magnetic Bragg peaks are present at the pseudo-M_1 (See Fig. S17) (½, 0, 3L±1), (0, ½, 3L±1) and (½, -½, 3L±1) locations. (Note that for the $R\bar{3}$ space group the symmetry conditions dictate every L±3 to be symmetry equivalent, which would naturally mean that we should only observe 3L+1 (L=integer) index peaks. However, a large crystal has 180° inverted domains which naturally leads to all 3L±1 index peaks for both the structural and magnetic orders. The presence of this inverted domain does not affect the following discussion of the 2-magnon spectrum.). At an in-plane magnetic field of 2 T, the M1 and Y points are rendered non-equivalent as the magnetic field breaks the in-plane mirror-symmetry. Magnetic Bragg peaks disappear at the BZ locations which are perpendicular to the field (See Fig. S1).

Above Bc1, the ZZ2 phase co-exists with the ZZ1 phase. Both the phases have magnetic Bragg peaks which are resolution limited [\cite Balz et al.] which indicates the formation of large domains. In the

ZZ2 phase, additional magnetic Bragg peaks appear at the additional pseudo-M_1 (See Fig. S1) (½, 0, 3L±0.5), (0, ½, 3L±0.5) and (½, -½, 3L±0.5) locations indicating a 6-layer order arising from a 2-layer antiferromagnetic unit-cell doubling of the 3-layer repeat period already present in $R\bar{3}$. Additionally, new magnetic Bragg peaks appear at (0, 0, 1.5) locations which is consistent with the unit-cell doubling. This also indicates that this pseudo-Γ point is a new zone-center from where sharp magnon branches are expected to disperse.

It is naturally expected that as a field is applied beyond B_{C2}, a sharp resolution-limited magnon mode would appear which would be gapless at B_{C2} and would slowly get lifted by the field. This is contrary to our observations - we did not observe such a sharp mode appearing from (0, 0, 1.5) at B_{C2}. A sharp mode below the continuum starts to coalesce only at higher fields above 8 T.

In the following, we examine more carefully whether the continuum excitations observed at the (0, 0, 1.5) location could be a multiparticle continuum from magnons related to ZZ1 and ZZ2 phases. A multiparticle continuum must obey the reciprocal space kinematic constraints $E_k = \sum_q \epsilon_{\{\omega,k-q\}} + \epsilon_{\{\omega,q\}}$ i.e., the multiparticle continuum is a sum of the magnon modes which constitute the spectrum. In the ZZ1 and ZZ2 phases such magnon modes are supposed to appear at and above the symmetry allowed M1 or Y locations (red circles in Fig S1). Any (ω, $+q$) magnon branch can kinematically sum up with its corresponding (ω, $-q$) branch to create a 2ω multimagnon spectrum at the 3D Γ-point (0, 0, 0) location.

We note here that the continuum we observed was present at all q locations, and especially at (0, 0, 1.5). Magnons arising from ZZ1 will have a minimum at the integer-L locations. Thus, within the ZZ1 phase a basic 2-magnon continuum can only appear and show a minimum at integer L locations. The scenario observed by us are hence antithetical to the basic 2-magnon scenario.

We can similarly consider the situation with the ZZ2 phase with ½ integer L magnetic Bragg peaks: a two-magnon scenario involving two ZZ2 magnons leads to a continuum of scattering and a minimum at the integer L locations. Thus, we find that there are no simple kinematic avenues to create a 2-magnon continuum at (0, 0, 1.5).

Another possibility is a 2-magnon continuum which arises from a mixture of ZZ1 and ZZ2, where the magnon scattering at the (H, K, L±1) indices could kinematically add with the magnon scattering from the ZZ2 phase at (-H, -K, L±0.5) locations to ultimately lead to a scattering continuum at (0, 0, 1.5). While this is not impossible, it is still odd to imagine that ZZ1 + ZZ2 scattering would dominate the spectrum over a simpler ZZ1 + ZZ1 or ZZ2 + ZZ2 2-magnon scattering processes. Overall, if a 2-magnon spectrum is present, the most likely scenario would be a gapped minimum at the integer L locations.

The $R\bar{3}$ space group indicates that L±3 locations are symmetry equivalent, which would mean that magnetic Bragg peaks at locations (1/2, 0, 3L-1) is equivalent to (-1/2, 0, 3L'+1) and (1/2, 0, 3L+2) that would lead to a scattering continuum at (I', 0, 3I) locations where L, L' , I and I' are all integers. Hence the most likely location where we should have noticed excess scattering would be the (0, 0, 3) which is a high-symmetry point in $R\bar{3}$ space group with an allowed Bragg peak, and truly representative of the 2D Γ-point. Our slices along the out-of-plane L directions show that this is not the case, precluding any simple multimagnon scenarios.

The L-dispersion and the minima at (0, 0, 1.5) indicate an overall antiferromagnetic inter-layer coupling playing some role in the overall Hamiltonian and the spinon dispersions, which needs to be taken into account in future theories alongside the in-plane Kitaev interactions to reproduce the observations in this manuscript.

Supplementary References:

[1] Banerjee, Arnab, et al., npj Quantum Materials 3.1 (2018): 8.
[2] Sears, Jennifer A., et al., Physical Review B 95.18 (2017): 180411.
[3] Balz, Christian, et al., Physical Review B 103.17 (2021): 174417.
[4] Do, Seung-Hwan, et al., Physical Review B 106.6 (2022): L060408.
[5] Balz, Christian, et al., Physical Review B 100.6 (2019): 060405.
[6] Tanaka, O., et al., Nature Physics 18.4 (2022): 429-435.